Deep Space One Investigations of Ion Propulsion Contamination: Overview and Initial Results

D. Brinza, J. Wang, J. Polk, M. Henry

Jet Propulsion Laboratory, California Institute of Technology, Pasadena, CA 91109

1. Introduction

NASA's New Millennium Deep Space One (DS1) is the first interplanetary spacecraft operated on solar electric propulsion. The DS1 spacecraft was launched on October 24, 1998. Using a 30cm diameter Xenon ion thruster as its primary propulsion system, DS1 successfully flew by asteroid 9969 Braille on July 28, 1999, and is currently on a trajectory for possible encounters with comets Wilson-Harrington and Borrelly in 2001. A primary objective of DS1 is to flight validate solar electric propulsion for interplanetary science missions, including the characterization of ion propulsion induced interactions and contaminations, and their effects on spacecraft payloads, subsystems, and solar wind measurements.

It has long been recognized that ion thruster operation may lead to a variety of interactions and contaminations, and hence both science and engineering concerns have been raised. One may loosely classify ion propulsion induced environments as plasma environment, contamination environment, and field environment. The induced plasma and contamination environments are due to the continued presence of an exhaust plume, which is composed of both propellant efflux and non-propellant efflux. In ion thrusters, propellant ions are accelerated electrostatically by a system of grids to form a high velocity beam (typically with an energy of about 1 KeV). Electrons are emitted from a neutralizer for neutralization of the ion beam. The propellant that remains un-ionized also flows out of the thruster exit at a thermal speed corresponding to the thruster wall temperature ($\sim$ 500 K). Charge-exchange collisions will occur between the fast moving propellant ions and the slow moving neutrals which generate slow moving ions and fast moving neutrals. Hence, the propellant efflux consists of beam ions, neutralizing electrons, and a low energy charge-exchange plasma generated within the plume. The non-propellant efflux comes from the material sputtered from thruster components and the neutralizer. Impingement by the charge-exchange ions generated within the grids and downstream will lead to gradual sputtering of the accelerator grids, eventually leading to mechanical failure of the grid structure. The sputtered grid material is ejected as neutral atoms in the general direction of the plume. However, a fraction of the sputtered particles will also become ionized due to charge-exchange collisions with the propellant ions or electron impact ionizations. It is well known that both the propellant charge-exchange ions and the ionized sputtered particles can be pushed out of the plume by local electrostatic potential and backflow to interact with spacecraft. The induced field environment is primarily due to the static electric and magnetic fields of the thruster and electromagnetic noises generated by the thruster during operation. The interaction of the plasma plume and the ambient plasma environment may also generate electrostatic and electromagnetic fluctuations.

DS1 investigations of ion propulsion plasma environment are reported recently by *Wang et al.*[1999]. The investigations of the field environment will be reported in [*Henry et al.*,2000]. The objective of this paper is to study ion propulsion induced contaminations based on in-flight observations from DS1.

The DS1 thruster uses Xe, an inert gas, as its propellant. Therefore, the backflow of charge-exchange Xe ions will affect the spacecraft's plasma environment and space plasma measurement performed on-board, but will not cause contaminations. On the other hand, the grid material of the thruster accelerator grid is molybdenum. The sputtered molybdenum species presents a serious contamination hazard due to molybdenum's low vapor pressures.

Ion thrusters have never been flown on an interplanetary spacecraft. Although ion thruster induced interaction has been a subject of extensive experimental and theoretical studies(for example, see *Jones et al*[1970], *Carruth*[1981], *Samanta Roy et al.*[1996a,b], *Wang et al.*[1996], *Katz et al.*[1997], and references therein), there have been no comprehensive in-flight investigations due to lack of flight opportunities. While in-flight investigations have been attempted on the SERT II spacecraft[*Kerslake et al.*,1971] in a polar or-

bit for a mercury ion thruster and on the ATS 6 spacecraft[*Worlock et al.*,1971] in geosynchronous orbit for a cesium ion thruster, almost all existing experimental data on ion thruster contaminations are obtained from ground tests of ion thrusters, with the majority of the data obtained for mercury and cesium ion thrusters [*Carruth*, 1981; *Jones et al*, 1970]. The DS1 mission provides the first ever comprehensive in-flight investigations of ion propulsion induced interactions and their effects.

This paper reports initial analysis of the first in situ measurements of ion propulsion induced contamination environment obtained from an interplanetary spacecraft. Section 2 describes the DS1 ion thruster and instrumentation. Sections 3 presents results from in-flight contamination measurements. Section 4 discusses a preliminary analysis of thruster grid erosion and the contamination environment. Section 5 contains a summary and conclusions.

2. Ion Thruster and Diagnostics Instruments

NSTAR Ion Propulsion System

The DS1 spacecraft is illustrated in Figure 1. A detailed description of the spacecraft can be found in [*Rayman and Lehman*, 1997].

The flight ion propulsion system (IPS) is developed under the NASA Solar electric propulsion Technology Application Readiness (NSTAR) program, a joint Jet Propulsion Laboratory/Glenn Research Center effort with industry participations from Hughes Electron Dynamics (HED), Moog Inc., and Spectrum Astro, Inc. The 30 cm diameter xenon NSTAR ion thruster, fabricated by HED, is designed to operate over an input power range of 0.5–2.3 kWe with a thrust of 20–92 mN, a specific impulse of 1950–3100 s, and a total beginning-of-life efficiency of 0.42–0.62. The propellant Xe^+ ions are accelerated through a molybdenum grid to form a beam with an energy of up to 1100 eV (exit beam velocity of $v_b \simeq 3.5 \times 10^6$ cm/s). and a current of up to 1.8 A. A detailed description of the NSTAR ion propulsion system and its in-flight validation is discussed in [*Polk et al.*,1999a].

Ion Propulsion Diagnostics Subsystem

DS1 carries two science instrument packages: the Miniature Integrated Camera and Spectrometer (MICAS) and the Plasma Experiment for Planetary Exploration (PEPE), and one ion propulsion diagnosis package: the Ion propulsion Diagnostic Subsystem (IDS). Ion propulsion related investigations are primarily based on IDS measurements.

The Ion Propulsion Diagnostic Subsystem is an integrated, comprehensive set of diagnostics designed to characterize ion propulsion induced environments and contaminations. IDS has two interconnected hardware units: the Diagnos tics Sensors Electronics Unit (DSEU) and the Remote Sensors Unit (RSU), and integrates a suit of 12 diagnostic sensors as shown in Figure 2. The contamination and plasma sensors are mounted on the RSU and the field sensors are mounted on the DSEU. The contamination monitors include two quartz crystal microbalance (QCM) and calorimeter pairs. Plasma measurements are made by a retarding potential analyzer (RPA), a planar Langmuir probe (LP), and a spherical Langmuir probe. Electrostatic and electromagnetic noise measurements are made by a plasma wave antenna and a search coil magnetometer. Magnetic field measurements are made by two flux gate magnetometers. The two flux gate magnetometers are provided by the Technical University of Braunschweig, and the plasma wave antenna is provided by TRW. The rest of the sensors are built at JPL.

This paper will focus on in-flight measurements obtained from IDS contamination monitors, which are located at a distance of 75cm from the ion thruster beam centerline. The two QCM and calorimeter pairs are used to characterize mass deposition rates and contamination effects on surface thermo-optical properties. The QCMs detect mass variations on the sensor surface via the induced frequency change in the oscillating quartz crystal sensor. The calorimeters provide indirect knowledge of solar absorptance and hemispherical emittance by temperature measurement of the thermally isolated sensor surface.

One pair of sensors is oriented as to have a direct line-of-sight view of the NSTAR ion engine. This pair will be called QCM0. The angle between QCM0 and the ion thruster beam centerline is about 85^o. The other contamination monitor pair is shadowed from direct view of the NSTAR engine by the DS1 propulsion module assembly. This pair will be called QCM1.

Each QCM provides very high sensitivity measurement (< 10 ng/cm^2) of mass accumulation on the sensor. The long-term drift of the QCM should not exceed 50 ng/cm^2 per month, which corresponds to a minimum detectable molybdenum deposit rate of 1 monolayer per year. Temperature changes and solar illumination of the sense crystal affect QCM response. For substantial mass accumulation, the temperature and solar illumination effects on the QCM measurement are minor.

The calorimeters can determine solar absorptance changes to better than 0.01 and emissivity changes to better than 0.01. The calorimeters use the sun as a

stimulus for determination of solar absorptance. The calorimeters include a control led heater to permit measurement of the hemispherical emissivity of the surface. Spacecraft surfaces in the field of view of the calorimeter complicate data analysis because of the uncertain heat loads that these surfaces provide to the sensor surface.

The QCM0 pair is expected to accumulate readily detectable amounts of sputtered molybdenum. On the other hand, the deposition rate on non-line-of-sight surfaces is expected to be very low since only the ionized particles can backflow to reach the non-line-of-sight surfaces from thruster downstream. Hence, the QCM1 measurements are expected to be dominated by the ionized molybdenum particles and/or contamination from the spacecraft and launch environments.

3. In-flight Contamination Measurements

The contamination monitors have functioned properly, and have produced high quality data for assessing the contamination environments on DS1. The IDS QCM sensors are 10 MHz fundamental frequency devices, hence the frequency to area mass density conversion is 4.43 ng/cm^2Hz. QCM beat frequencies are sensitive to changes in temperature and solar illumination of the sense crystal. In order to extract low-level contamination information, QCM data often must be corrected for temperature and solar illumination. The magnitude of the IPS-induced contamination for the line-of-sight (QCM0) sensor is such that these corrections are not necessary. The non-line-of-sight (QCM1) sensor, though, had significantly less accumulation and therefore its data should be corrected prior to precise quantitative interpretation. The data, as presented in this paper, have not been corrected for sense crystal temperature or solar illumination.

The data from the QCM and calorimeter sensors are reduced, analyzed and correlated with NSTAR ion engine operations. The preliminary results are discussed chronologically in this section. In this paper, rates of contamination accumulation during IPS thrusting are conveniently expressed in terms of Angstroms of molybdenum per 1000 hours of operation: A/kHr.

Measurements During Launch Operations

The final pre-flight functional test of the IDS prior to launch was conducted on DOY 293-1998. Data from the QCMs provide the pre-launch baseline for assessing launch-phase contamination in the vicinity of the DS1 to launch vehicle interface. The pre-launch readings were obtained at 16C and are 2475 Hz and 2085 Hz for QCM0 and QCM1 respectively. Following launch, DS1 was oriented with the sun vector aligned with the spacecraft X-axis. In this orientation, QCM0 is illuminated with a sun angle of approximately 46, whereas QCM1 is in the shadow of the DS1 propulsion module. The IDS was not activated until 1998-298 at 2201 hours (approximately 34 hours after launch). The initialization of IDS included a special activity ("DFrost") intended to bake-off volatile contamination from the QCMs and calorimeters by heating the sensors to +75C. Very little change (< 50 Hz) was observed in the beat frequency of either QCM as a result of the initial post-launch DFrost.

The frequencies and temperatures for QCM0 and QCM1 just prior to DFrost were 2260 Hz (at +30 C) and 2272 Hz (at +16C) respectively. Since QCM0 was exposed to the sun after launch, it is suspected that most of the contaminants accumulated on it were evaporated prior to IDS initialization. The beat frequency for QCM1 increased by 187 Hz from pre-launch to IDS initialization, yielding an estimated 0.8 $\mu g/cm^2$ (80A) accumulation for launch phase contamination. This accumulation was not affected by the DFrost activity but was removed when DS1 rotated to expose the NSTAR ion engine to the sun (NSTAR Decontamination Maneuver). Figure 3a shows the early mission response of QCM1 to the DS1 orientation with respect to the sun shown in Figure 3b. Note the substantial frequency and temperature changes near DOY 304-1998 associated with the NSTAR Decontamination Maneuver. There is an additional turn on DOY 305-1998, which further affects the QCM1 frequency and temperature. On DOY 306-1998, DS1 returned to the nominal sun on X-axis orientation. Using the frequency reading at this time, it appears that about a 165 Hz change had occurred as a result of this solar-stimulated bakeout. Based on this interpretation of QCM1 data, it appears that the RSU surfaces were contaminated with approximately 80A of low-volatility organic material most of which was removed upon exposure to the sun.

Measurements During IPS Operations

The QCM data for the IPS operations of the first year of flight for DS1 are illustrated on Figures 4a through 4g. The figures are arranged so the response of the line-of-sight (QCM0) and non-line-of-sight (QCM1) sensors can be compared side-by-side. The four pairs of figures represent time intervals during which IPS operations of substantial duration occured. Data for minor thrusting events and the trajectory correction maneuvers prior to the Asteroid Braille encounter do not show significant accumulations on either QCM. Similarly, data for the long, non-thrusting intervals are not shown since no accumulation occured on either QCM in these periods. To correlate these measurements with NSTAR ion engine operations, the NSTAR throttle table is listed in Table

1. In the following discussions, the mission levels (ML) listed in Table 1 will be used in all references to IPS operations.

The first period of extended IPS operations occurred from DOY 328-1998 to DOY 005-1999. The line-of-sight sensor (QCM0) response is shown in Figures 4a and 4c, while the shadowed sensor (QCM1) response is seen in Figures 4b and 4d. The initial IPS operations consisted of 10 days thrusting with the thrust vector essentially Earth-pointed. During these initial operations, the NSTAR engine was first operated at low-thrust (Mission Levels 6 to 27) for five days. During this period, QCM0 frequency increased by 123 Hz while QCM1 increased by 25 Hz. In order to determine the deposition rate for Mission Level 27 (ML27), a least squares fit of the frequency data for the 117 hour interval starting on DOY 329-1998 and ending on DOY 334 was performed. The resulting slope in units of Hz/day was converted to A(Mo)/kHr by multiplying by 1.804.

QCM0 data for the remaining thrusting of the initial period shows some interesting features. On DOY 338-1998, DS1 performed a turn to orient the thrust vector from Earth-pointed to the desired mission trajectory thrust attitude. Note that the molybdenum deposition rate for QCM0 at ML83 prior to DOY 338-1998 was 88 A/kHr, whereas after the turn, the deposition rate increased to 197 A/kHr. It is not yet known whether this rate change is due to thermal effects on the NSTAR ion engine grids. There have been no reports of change in mass sensitivity with varying sun angle on QCMs, so it is unlikely that the rate change is an instrument artifact.

Following the turn to thrust attitude, DS1 continued thrusting until DOY 342-1998. Other technology activities, including initial turn-on of the Plasma Experime nt for Planetary Exploration (PEPE) instrument were performed. On DOY 346-1998, IPS was restarted at low thrust level (ML6) to assess effects on the PEPE instrument. The on-board sequence raised the IPS thrust level to ML85 after 15 minutes. The available power for IPS thrusting was overestimated, resulting in a DS1 "safe-mode" transition. IPS thrusting resumed on DOY 348-1998 after DS1 spent two days in safe-mode.

The first IPS thrust segment ended with two weeks of essentially continuous thrusting with the thrust levels gradually decreasing from ML78 on DOY 352-1998 to ML 72 on DOY 005-1999. During this interval, the DS1 on-board navigation software would update the thrust vector and level at 12-hour intervals. The IPS thruster was turned off at 1600 hours on DOY 005-1999. The deposition on QCM0 steadily increased over this interval, except for a brief interval on DOY 356-1998 where DS1 re-oriented to place the sun on the X-axis for approximately 3 hours. QCM1 also showed consistent frequency increase, although an order-of-magnitude lower than that for QCM0. The thrust segment continued into early 1999. With st eady accumulation by both QCMs witnessed in Figures 4c and 4d. Subsequent to engine turn-off on DOY 005-1999, DS1 performed maneuvers to characterize stray-light into the MICAS imager. The effect on QCM1 (100 Hz oscillation) due to shadowing of minor sun-angle changes caused by attitude control system dead-banding is quite evident for DOY 009-1999 through DOY 012-199.

The next major IPS thrust interval was the C1A and C1B activities performed from DOY 075-1999 until DOY 117-1999. This thrusting was performed with weekly optical navigation (OpNav) activities and high-rate telemetry downlink intervals. Thrusting duty cycle was typically greater than 90% during this interval. The OpNav/downlink events are readily identified in Figures 4e and 4f by 100 Hz frequency dips in both QCM0 and QCM1 as well as 60 temperature increases for both sensors. The deposition rates for QCM0 are labeled in Figure 4e with time averaged thruster mission levels for each thrust segment. During the C1A and C1B activities, the on-board navigator varied the IPS thruster power. The DS1 power management software would monitor battery state-of-charge and perform thrust reduction as required. For this period, the non-line-of-sight sensor accumulated only about 1% of the amount of molybdenum collected by QCM0.

Subsequent to the Asteroid Braille encounter on DOY 210-1999, IPS operated for an interval of almost 12 weeks. As the DS1 sun distance decreased, the mission level gradually increased during the C2A and C2B segments. The deposition rates of both QCMs also increased during this period as seen in Figures 4.5g and 4.5h. The brief, periodic spikes in the QCM frequency data occur at each of the weekly OpNav and downlink sessions, again caused by sun angle changes. The accumulation of molybdenum on the shadowed QCM is about 5% of that witnessed by the line-of-sight sensor.

The four thrusting segments shown in Figures 4a through 4h account for over 95% of the IPS operating time for the first year of the mission. Of the 250A of molybdenum collected on the line-of-sight QCM0 in the first year of operation, almost 95% of the accumulation are shown in these figures. The shadowed QCM1 only collected the equivalent mass of a 25A thick deposit of molybdenum in the first year, or approximately 10% of molybdenum deposited on the line-of-sight sensor. The source of this non-line-of-sight contaminant is attributed to ionized molybdenum, moving along trajectories affected by electrostatic potentials associated with

the thruster plume and spacecraft surfaces. However, it is possible that a portion of the deposited mass on the shadowed QCM is not molybdenum, perhaps from general spacecraft outgassing contamination.

Correlation with IPS Operations

The deposition rate averaged over the entire IPS operating time for the first year of the mission is 90A/KHr and about 9A/KHr for QCM0 and QCM1 respectively. However, the deposition rate differs significantly at different thrusting levels. The deposition rates for QCM0 and QCM1 averaged for each thrusting segment after the first 9 days of operations are summarized in Figure 5 as a function of NSTAR mission levels. Most of the thrustings were performed at ML32 through ML45. A few thrusting segments were performed at ML74 through ML83. Note that the accelerator grid voltage is at -150V for thrusting levels below ML56 and at -180V for thrusting levels above ML56. Due to the IPS operations profile, there is no data available for mission levels 50 through 70.

As indicated before, the line-of-sight QCM0 accumulates molybdenum at a substantially higher rate than the shadowed QCM1. The line-of-sight sensor deposition rate appears roughly proportional to the mission level whereas the non-line-of-sight rate seems more strongly affected by mission level. The QCM1 data suggests that there seem to be threshold in between ML50 and ML70. The deposition rates is near zero at mission levels below ML50 and jumps to O(10) A/KHr at mission levels above ML70.

Since the amount of the sputtered Mo particles is directly related to accelerator impingement, in Figure 6 we plot the QCM0 deposition rate against the measured accelerator grid impingement current. Since the electrostatic potential with the plume will have a strong effect on the trajectories of the ionized Mo particles, in Figure 7 we show the QCM1 deposition rate against the ion beam current. These results will be discussed in Section 4.

Comparison with Ground Test Results

It is also interesting to compare in-flight measurements with ground test measurements obtained during the NSTAR 8000-hour Life Demonstration Test (LDT) performed at JPL.

During LDT, the NSTAR ion engine was operated at the full power, 2.5 kW, for 8000 hours. The LDT contamination monitors were mounted on a curved support beam at 120cm from the engine, and were placed at angles from 40^o to 110^o from the thrust axis at 10^o intervals. Recall that on DS1, the line-of-sight QCM0 is located at 75cm from the thruster centerline, 85^o off thrust axis. At the end of LDT, the molybdenum deposition at the 85^o off thrust axis position is found to be about 500 A/kHr, and the average deposition rate is about 62.5 A/kHr. Even though the grid is an extended source, the deposition thickness is roughly inversely proportional to square of distance from grids. Hence, the expected deposition rate for an LDT witness monitor in the equivalent position of the line-of-sight QCM0 is 160 A/kHr. This result is comparable to the in-flight QCM0 deposition rate for high mission levels (see Figure 5).

4. Discussions

The results from diagnostics sensors are useful from two perspectives. First, the in-flight data provides a spacecraft systems engineer information for modeling environments on future spacecraft. Second, the data, when correlated with ground test, can help assess ion engine health because contamination measurements can provide an indication of grid wear. This section presents a preliminary analysis of both the contamination environment and ion thruster grid erosion rates.

Assumptions

IDS makes only single point measurements. We can use the measured deposition rates to infer the contamination environment as well as grid erosion rates with a suitable model describing the flux of eroded material from the grid surface. However, such a process typically requires one to invoke several key assumptions.

Ground experiments and computational modeling have shown that grid sputtering is primarily caused by propellant charge-exchange ions [*Peng et al.*,1993; *Polk et al*,1999b; *Crofton and Boyd*,1999; and references therein] Because of its negative bias voltage, charge-exchange ions generated within the aperture holes and on the upstream and downstream faces of the accelerator grid can impinge upon the grid surface. The grid impingement process as well as detailed surface physics for molybdenum sputtering by Xe^+ are still subjects of ongoing research.

A commonly used assumption is to model the flux of sputtered particles as a cosine distribution that falls off as $1/R^2$ from a single point source in space and as a Maxwellian distribution in energy[*Samanta Roy et al.*,1996a]. This assumption will also be used in the analysis presented here. However, ion sputtering measurements have shown that the angular distribution of the sputtered atoms often changes with the energy of impinging ions and the energy distribution typically has a broader energetic tail[*Duchemin*,1999]. In particular,

data from ground testing has shown that the accelerator grid mass loss is peaked on the centerline of the engine [*Polk et al.*,1999b], so the flux of sputtered material may be approximated by that produced from a point source located on the grid in the center. The flux of sputtered molybdenum is assumed to be distributed according to the cosine of the ejection angle relative to the thruster axis. This is an approximation which must be verified with additional modeling. Material sputtered from planar targets has been found to follow an angular distribution given by the cosine of the ejection angle raised to a power ranging from 0.5 to 2, depending on the ion and target materials and bombarding energies [*Behrisch and Wittmaack*,1991]. The geometry of erosion on the accelerator grid is much more complex, however. There are two major erosion sites–the walls of the apertures in the grid and the downstream surface, where material is removed in a hexagonal pattern of pits and grooves surrounding each aperture [*Polk et al.*,1999b]. With this geometry, the angular distribution of sputtered material may be much more complicated than a simple cosine distribution.

Grid Erosion Rates

With the assumption that the flux of sputtered particles follow a simple cosine distribution that falls off as $1/R^2$, the molybdenum deposition rate γ_{Mo} on a surface located a distance R from the source is given by

$$\gamma_{Mo} = S\frac{\cos\theta_e \cos\theta_i}{2\pi R^2}. \quad (1)$$

where S is the source strength in mass ejected outward from the grid per unit time, θ_e is the ejection angle (the angle between the line joining the source and the deposition site and the thruster centerline), and θ_i is the incident angle between the sputtered atom trajectory and the deposition site surface normal. The source strength S calculated from the measured deposition rate γ_{Mo} on QCM1, plotted on the right hand axis in Figure 6, ranges from about 2 to 10 μg/khr.

These results can be compared to the source strength calculated from the expected grid erosion rate based on the measured grid impingement current. The relationship between the source strength and the erosion rate is given by

$$S = \lambda_e E_r = \lambda_e \lambda_y J_a Y M_{Mo}/e, \quad (2)$$

where E_r is the total mass loss per unit time from the grid and λ_e is the fraction of eroded material which is ejected away from the thruster. The second expression represents a model relating the erosion rate to the measured impingement current J_a [*Polk et al.*,1999b]. Y is the sputter yield for xenon ions striking the grid at normal incidence with an energy of 200 eV. Most of the ions impinging on the grid are assumed to be from the downstream charge exchange plasma and are accelerated through a voltage of up to 200 V as they fall from the beam potential on the centerline to the accelerator grid [*Polk et al.*,1999b]. M_{Mo} is the mass of a molybdenum atom and e is the charge on an electron. The factor λ_y represents deviations in the true mass loss from that expected from measured values of impingement current and published sputter yields, which may be due to values of incident energy greater than or less than 200 eV, redeposition of sputtered material, ground test effects which artificially reduce the sputter rate, etc. Data from the 8200 hour Life Demonstration Test suggest that λ_y may be as low as 0.22 [*Polk et al.*,1999b]. Data from this test were also used to estimate the value of λ_e at approximately 0.75. The dashed line in Figure 6 is the source strength based on these values.

The source strength inferred from the flight QCM0 measurements is approximately 6-7 times higher for impingement currents less than 3 mA and 12-15 times higher for the higher impingement currents. Much better agreement with the lower impingement currents is obtained with $\lambda_y = \lambda_e = 1$, as shown by the solid line in Figure 6.

The data at the low- and mid-power levels suggest a linear relationship between erosion or deposition rates and the impingement current, as expected from the model. However, the higher throttle levels (with impingement currents of about 4 mA) appear to deviate from this trend. These data were measured early in the flight, and the erosion rate may have been higher than at later times because of direct ion impingement. Direct impingement of beam ions at an energy of 1100 eV on portions of the accelerator grid may occur early in the operation of an engine. As these parts of the aperture walls are eroded away, the direct impingement decreases and the erosion is dominated by charge-exchange ions. The higher initial erosion rate would not be captured by the model, which assumes that the bombarding ion energy is less than or equal to 200 eV.

The results using values of λ_y and λ_e from the ground test suggest either a model specification error or that the erosion rates in space are much higher than those measured in ground tests. The validity of the model was checked by comparing the source strength inferred from the deposition measurements performed in the LDT to that calculated from the measured average erosion rate E_r and the value of λ_e for the test. The model yields excellent agreement within 50°. At higher angles, the source strength inferred from the deposition measurements is substantially higher than that based on measured grid erosion rates. This suggests that the dis-

crepancy noted above is due to a misspecification of the angular distribution. The sputtered molybdenum flux appears to follow a cosine distribution for low ejection angles, but is much larger than cosine at higher angles. This may be due to the flux contribution from the aperture walls, which would be expected to peak at higher angles to the grid surface normal. More detailed modeling of the source function is required to infer the grid erosion rate from the flight data, which are measured at an angle of about 85° off thruster axis.

Contamination Environment

We next consider the distribution of ionized molybdenum particles. In this preliminary analysis, we first obtain the normalized density distribution of the sputtered molybdenum atoms assuming that the flux of sputtered particles follow a $R^{-2}\cos\theta$ scaling in space and a Maxwellian distribution in energy. We then derive the density magnitudes based on the measured deposition rate by QCM0 and estimate the molybdenum ionization rate in the plume. Since the density of ionized molybdenum particles is negligible compared to the propellant ion density, the presence of Mo^+ ions will not change the plasma environment. Finally, we trace the Mo^+ ions in the electric field surrounding DS1 to obtain the distribution of molybdenum ions.

The grid impinging Xe^+ ions have an average energy of 150–180eV, corresponding to the accelerator grid voltage. Ongoing studies found that the most probable ejection energy of molybdenum being bombed by 180eV Xe^+ ions is about 6eV (3470m/s) [*Duchemin*,1999]. We use the average deposition rate at QCM0 over the 3500 IPS operation hours as a benchmark. Under our assumptions, we find that the sputtered Mo density at QCM0 is about $4.6 \times 10^4 cm^{-3}$ and that at thruster exit is about $6.6 \times 10^6 cm^{-3}$ for the observed average QCM0 deposition rate of 90A/kHr.

The sputtered Mo can become ionized due to charge-exchange with the propellant Xe^+ ions or electron impact ionization. *Samanta Roy et al.*[1996] compared the measured ionization cross sections for molybdenum,and found that charge-exchange is the more important ionization mechanism if the electron temperature is less than about 2eV while electron impact ionization becomes more important if the electron temperature is larger than 2eV. We applied the same Mo^+ production rate model used in [*Samanta Roy et al.*,1996] The Mo^+ ions are traced in a plume model obtained from particle-in-cell simulations [*Wang et al.*,1996]. The calculations show that, corresponding to an average Mo deposition rate of 90A/kHr, the calculated Mo^+ density at QCM1 location would be about $10^4 cm^{-3}$ and the calculated Mo^+ flux would be on the order of 10A/kHr. This result seems to be consistent with QCM1 measurements for high mission levels.

Figures 5 and 7 show that the deposition rate at QCM1 jumps at higher mission levels. We offer two arguments to explain this observation. The first argument concerns the production rate of ionized molybdenum. This rate is expected to increase dramatically with mission level for the following reasons: 1) More sputtered molybdenum atoms are produced at higher mission levels due to increased impingement by charge-exchange xenon, 2) More beam ions are produced by the engine at higher mission levels, increasing the rate for charge-exchange ionization of molybdenum atoms, and 3) Higher electron temperatures are observed at higher mission levels, increasing the rate for electron impact ionization of neutral molybdenum. The second argument concerns the effect of plume potential on particle trajectories. [*Wang et al.*,1999] found that in order for a charged particle originated with the plume to backflow upstream, the potential difference between the plume and spacecraft must be sufficiently large. Hence, significant backflow of ionized molybdenum originated in the plume occurs only at high mission levels when the plume potential is significantly higher due to higher beam currents.

5. Summary and Conclusions

For the first time, a comprehensive in-flight investigation of ion propulsion contaminations is being carried out on an interplanetary spacecraft. The IDS has obtained high quality data on the contamination environment as a function of IPS thrust level. After about 2750 hours of IPS operation in the first year of the DS1 mission, the line-of-sight QCM0 has collected about 250 Angstroms of molybdenum and the non-line-of-sight QCM1 has only collected the equivalent mass of a 25 Angstroms thick deposit of molybdenum. The line-of-sight QCM0 deposition rate appears proportional to the mission level, ranging from about 33A/kHr at ML27 to about 200 A/kHr at ML83. The QCM0 deposition rate is consistent with ground measurements obtained during the NSTAR ion thruster 8000-hour life test. The non-line-of-sight QCM1 rate exhibits a step-function like behaviour, with deposition rates < 5A/kHr for mission levels below ML50 and > 20A/kHr for mission levels above ML70. The source of the non-line-of-sight contaminant is attributed to ionized molybdenum. QCM1 results suggest that significant Mo^+ backflow will occur only at high thrusting levels when the backflow is facilitated by a sufficiently large plume potential. Since the DS1 solar arrays do not extend into the line-of-sight zone, are well removed from the thruster (> 2 meters)

and are negatively grounded, the amount of molybdenum deposited on the SCARLET concentrator lenses is expected to be very small. Preliminary analyses of both the DS1 contamination environment and ion thruster grid erosion rates are also presented. Grid erosion rates inferred from QCM measurements and the commonly used $R^{-2}\cos\theta$ model for the sputtered molybdenum flux are found to be substantially higher than that based on measured grid impingement currents. More detailed modeling of grid sputtering is required to infer the grid erosion rate as well as the contamination environment from the flight data.

Acknowledgments

We acknowledge technical support provided by the DS1 mission and the NSTAR project. We acknowledge many helpful discussions with O. Duchemin and J. Brophy (JPL) I. Katz (Maxwell Labs), and R. Samanta Roy (IDA). This work was performed at Jet Propulsion Laboratory, California Institute of Technology, under a contract with NASA, and was supported by the NASA New Millennium Deep Space 1 mission and the NASA Solar Electric Propulsion Technology Application Readiness Project.

References

Behrisch, R. and K. Wittmaack Ed., Sputtering by particle bombardment III: characteristics of sputtered particles, technical applications, Springer-Verlag, Berlin, 1991.

Carruth, M., Ed., Experimental and analytical evaluation of ion thruster/spacecraft interactions, *JPL Publication* 80-92, 1981.

Crofton ,M. and I. Boyd, The origins of accelerator grid current: analysis of T5-grid test results,*AIAA Pap.* 99-2443, 1999.

Duchemin, O., private communications, 1999.

Henry, M., et al., NSTAR diagnostic package architecture and deep space one spacecraft event detection, to appear in *IEEE* Aerospace Conference, 2000.

Jones, S., J. Staskus, and D. Byers, Preliminary results of SERT II spacecraft potential measurements, *NASA TM X-2083*, 1970.

Katz, I., V. Davis, J. Wang, and D. Brinza, Electrical potentials in the NSTAR charge-exchange plume, *IEPC Pap.* 97-042, 1997.

Kerslake, W., R. Goldman, and W. Nieberding, SERT II: mission, thruster performance, and in-flight thrust measurements, *J. Spacecraft and Rockets*, 8(3), 1971, pp213.

Peng, X., W. Ruyten, and D. Keefer, Charge-exchange grid erosion study for ground-based and space-based operations of ion thrusters, *IEPC Pap.* 93-173, 1993.

Polk, J., et al., In-flight validation of the NSTAR ion thruster technology on the Deep Space One mission, *AIAA Pap.* 99-2274, 1999a.

Polk, J., et al., An Overview of the results from an 8200 hour wear test of the NSTAR ion thruster, *AIAA Pap.* 99-2446, 1999b.

Rayman, M. and D. Lehman, Deep Space One: NASA's first deep-space technology validation mission, *Acta Astronautica*, 41(4), 1997, pp289.

Samanta Roy, R., D. Hastings, and N. Gatsonis, Ion-thruster modeling for backflow contamination, *J. Spacecraft Rockets*, 33(4), 1996a, pp525.

Samanta Roy, R., D. Hastings, and N. Gatsonis, Numerical study of spacecraft contamination and interactions by ion-thruster effluents, *J. Spacecraft Rockets*, 33(4), 1996b, pp535.

Wang, J., J. Brophy, and D. Brinza, 3-D simulations of NSTAR ion thruster plasma environment, *AIAA Pap.* 96-3202, 1996.

Wang, J. et al, "Deep space 1 investigations of ion propulsion plasma environment", submitted to *J. Spacecraft Rockets*, 1999.

Worlock, R., E. James, R. Hunter, and R. Bartlett, ATS-6 cesium bombardment engine north-south stationkeeping experiment, *IEEE Trans. Aerospace and Electronic Systems*, ASE-11(6), 1975, pp1176.

Table 1: NSTAR Ion Thruster Flight Throttle Table

NSTAR Throttle Level	Mission Throttle Level	PPU Input Power (kW)	Engine Input Power (kW)	Calculated Thrust (mN)	Main Flow Rate (sccm)	Cathode Flow Rate (sccm)	Neutralizer Flow Rate (sccm)	Specific Impulse (s)	Total Efficiency
15	111	2.52	2.29	92.4	23.43	3.70	3.59	3120	0.618
14	104	2.38	2.17	87.6	22.19	3.35	3.25	3157	0.624
13	97	2.25	2.06	82.9	20.95	3.06	2.97	3185	0.630
12	90	2.11	1.94	78.2	19.86	2.89	2.80	3174	0.628
11	83	1.98	1.82	73.4	18.51	2.72	2.64	3189	0.631
10	76	1.84	1.70	68.2	17.22	2.56	2.48	3177	0.626
9	69	1.70	1.57	63.0	15.98	2.47	2.39	3136	0.618
8	62	1.56	1.44	57.8	14.41	2.47	2.39	3109	0.611
7	55	1.44	1.33	52.5	12.90	2.47	2.39	3067	0.596
6	48	1.32	1.21	47.7	11.33	2.47	2.39	3058	0.590
5	41	1.19	1.09	42.5	9.82	2.47	2.39	3002	0.574
4	34	1.06	0.97	37.2	8.30	2.47	2.39	2935	0.554
3	27	0.93	0.85	32.0	6.85	2.47	2.39	2836	0.527
2	20	0.81	0.74	27.4	5.77	2.47	2.39	2671	0.487
1	13	0.67	0.60	24.5	5.82	2.47	2.39	2376	0.472
0	6	0.53	0.47	20.6	5.98	2.47	2.39	1972	0.420

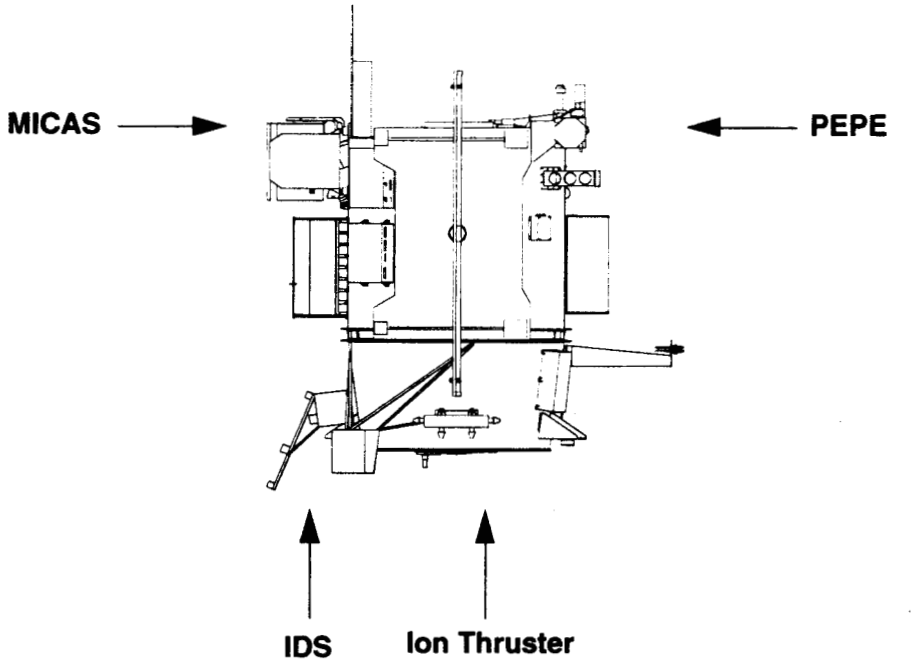

Figure 1 Illustration of the Deep Space 1 Spacecraft

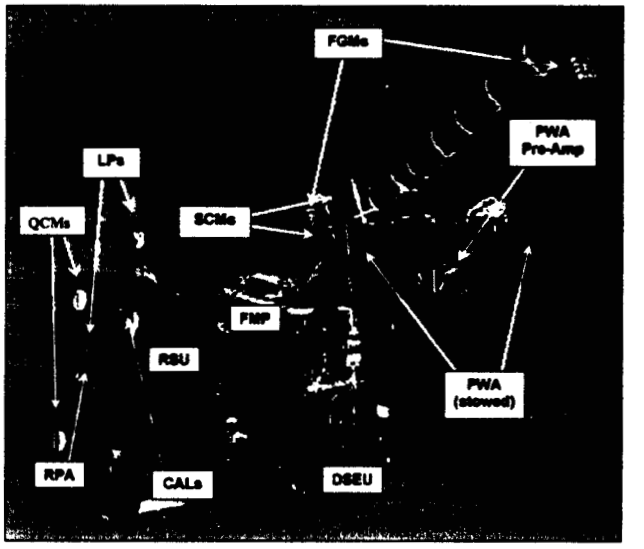

Figure 2: The Ion Propulsion Diagnostic Subsystem

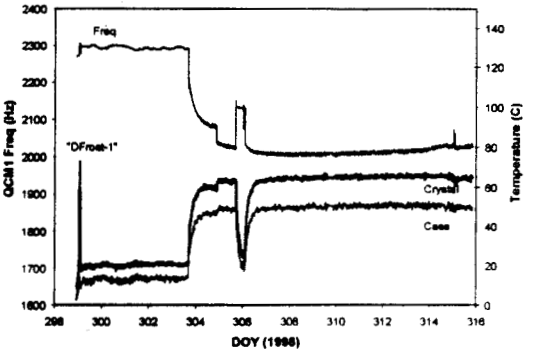

Figure 3a. QCM1 early mission response

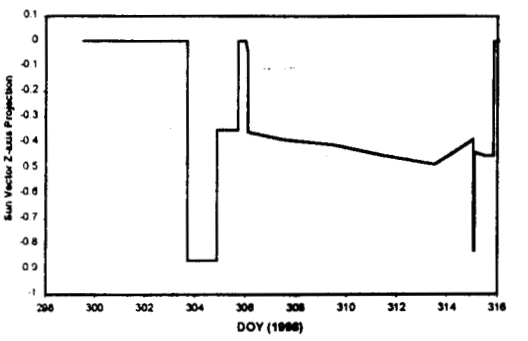

Figure 3b. Early mission DS1 sun orientation

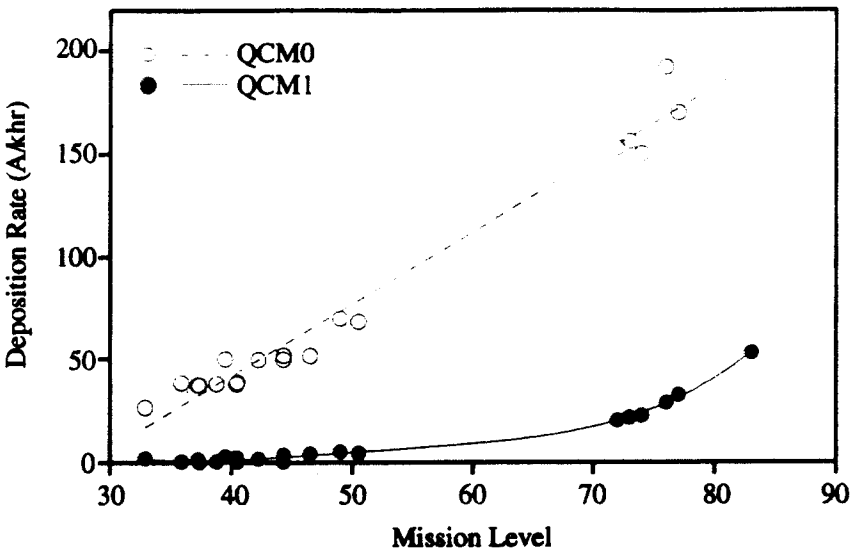

Figure 5: QCM0 and QCM1 deposition rates vs. mission level

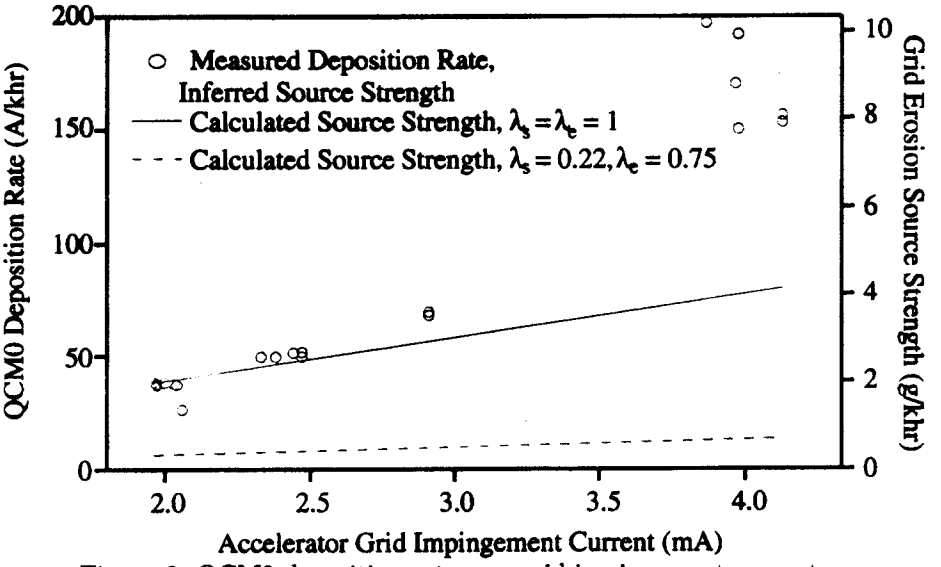

Figure 6: QCM0 deposition rates vs. grid impingement current

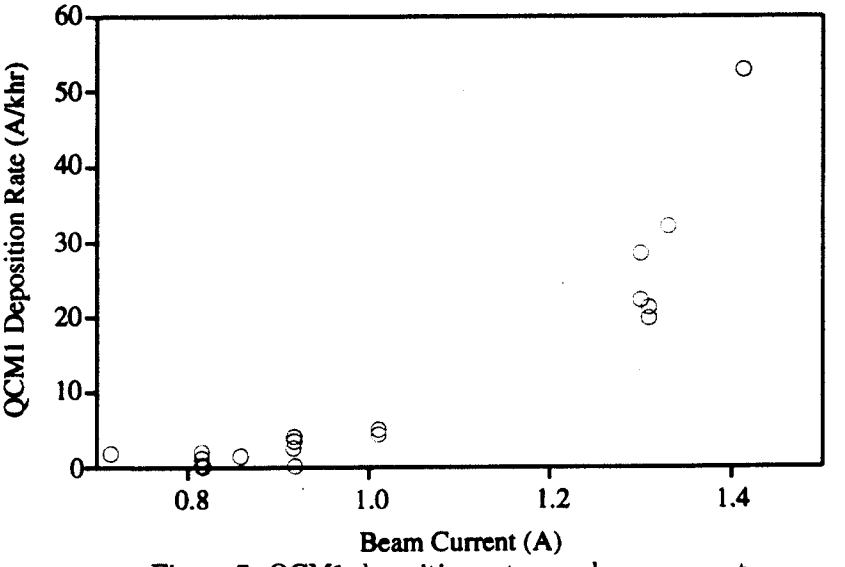

Figure 7: QCM1 deposition rates vs. beam current

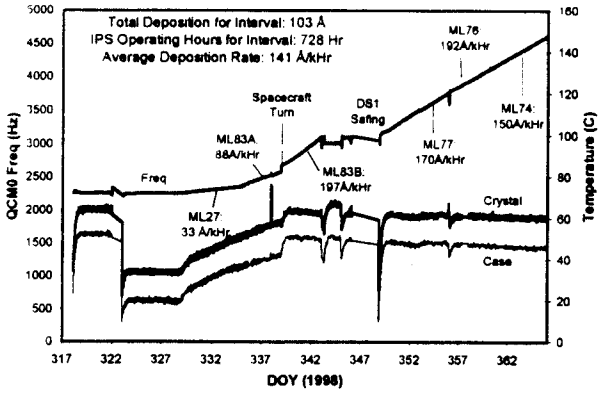

Figure 4a QCM0 data for 1998-317 through 1998-365.

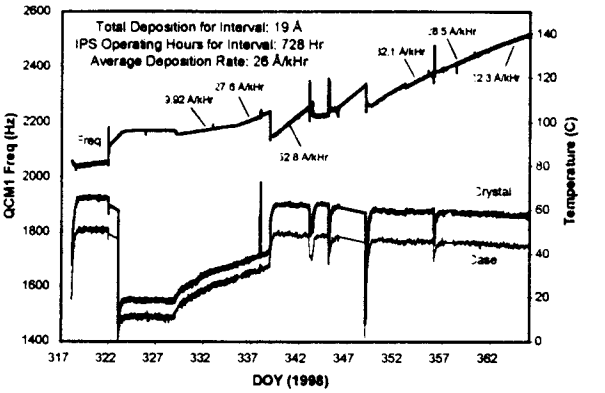

Figure 4b QCM1 data for 1998-317 through 1998-365.

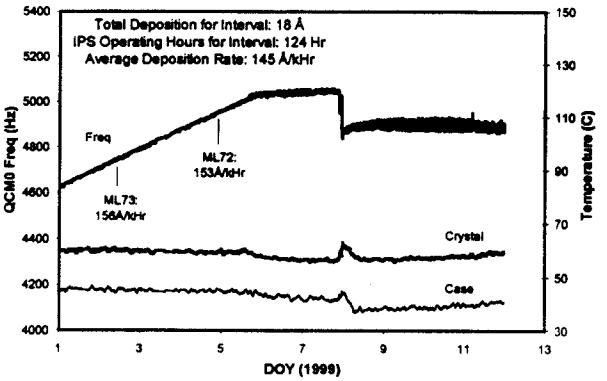

Figure 4c QCM0 data for 1999-001 through 1999-012.

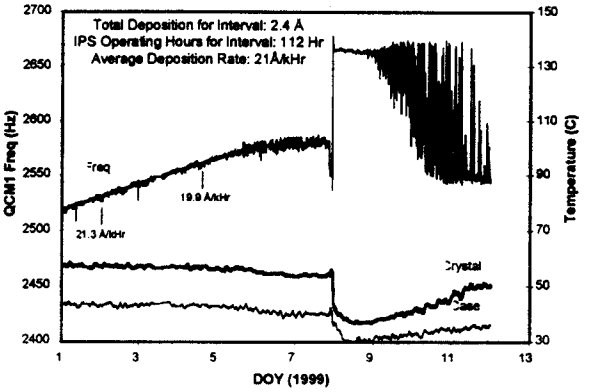

Figure 4d QCM1 data for 1999-001 through 1999-012.

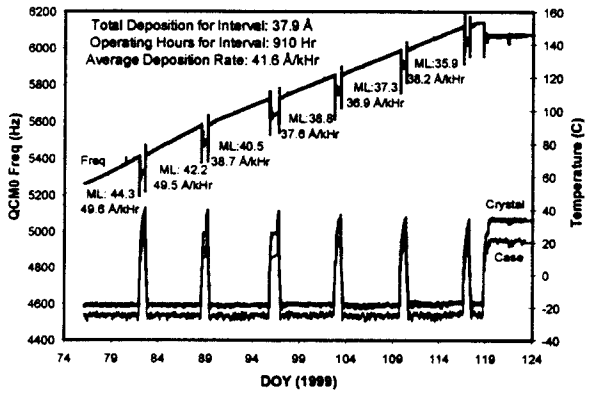

Figure 4e QCM0 data for 1999-074 through 1999-124.

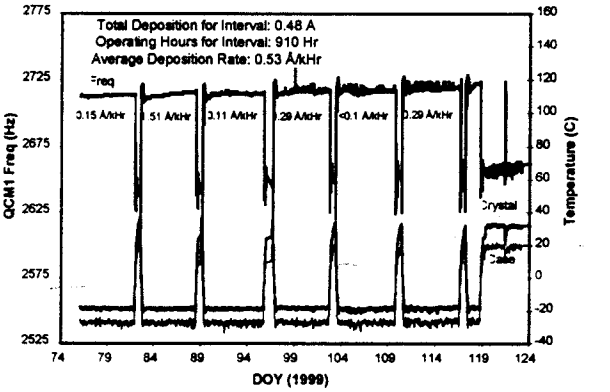

Figure 4f QCM1 data for 1999-074 through 1999-124.

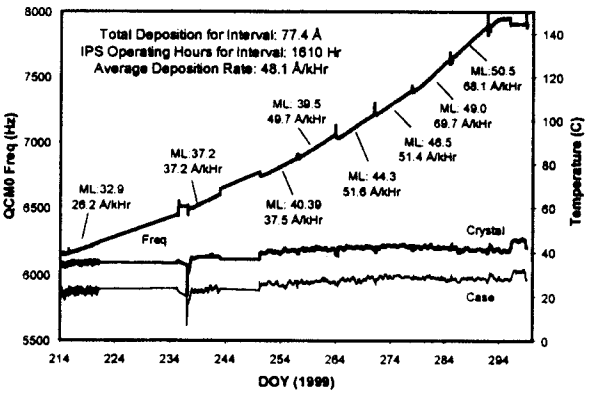

Figure 4g QCM0 data for 1999-214 through 1999-300.

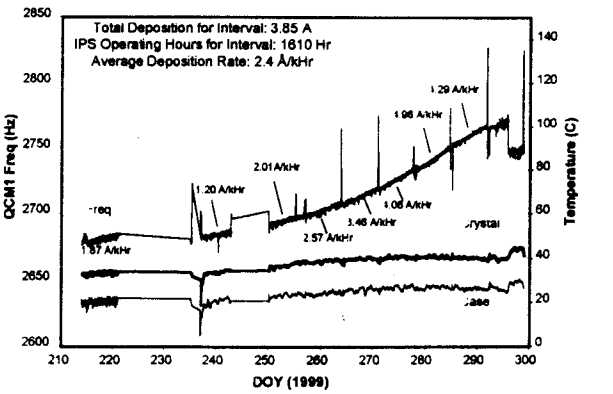

Figure 4h QCM1 data for 1999-214 through 1999-300.